Structural and physical properties of $SmFe_{1-x}Ir_xAsO$ ($0 \leq x \leq 0.275$) obtained by synchrotron x-ray diffraction, Raman spectroscopy, and magnetization measurements

Beatrice Maroni,[1] Lorenzo Malavasi,[1,*] M. Cristina Mozzati,[2] Marco S. Grandi,[2] Adrian H. Hill,[3] Daniele Chermisi,[4] Paolo Dore,[5] and Paolo Postorino[4]

[1]*Dipartimento di Chimica Fisica "M. Rolla," INSTM (UdR Pavia) and IENI-CNR, Università di Pavia, Viale Taramelli 16, 27100 Pavia, Italy*

[2]*CNISM, Unità di Pavia and Dipartimento di Fisica "A. Volta," Università di Pavia, Via Bassi 6, I-27100 Pavia, Italy*

[3]*European Synchrotron Radiation Facility, BP 220, F-38043 Grenoble, France*

[4]*CNR-IOM and Dipartimento di Fisica, Università di Roma "La Sapienza," P.le A.Moro 2, 00185 Rome, Italy*

[5]*CNR-SPIN and Dipartimento di Fisica, Università di Roma "La Sapienza," P.le A.Moro 2, 00185 Rome, Italy*

(Received 2 June 2010; revised manuscript received 10 August 2010; published 2 September 2010)

In this paper we have carefully investigated the structural and physical properties of the $SmFe_{1-x}Ir_xAsO$ solid solution ($0 \leq x \leq 0.275$), chosen as a case study, by means of synchrotron x-ray diffraction, Raman spectroscopy, and magnetization measurements. Our data confirm the positive role of doping in terms of insurgence of superconductivity for $x \geq 0.06$. Increasing of doping leads to the disappearance of superconductivity while preserving the tetragonal structure and As-Fe(Ir)-As bond angles within the range where superconductivity should be observed. The set of data collected in this paper have been used together with available literature results on similar transition-metal-doped *RE*FeAsO (*RE*=rare earth) compounds in order to try to understand and explain the peculiar behavior of these phases and their phase diagrams. We provided a solid explanation of the observed trends and features by considering the compressibility along the *c* axis of the crystal structure as the key parameter in transition-metals-doped iron pnictides.

DOI: 10.1103/PhysRevB.82.104503 PACS number(s): 74.25.−q

I. INTRODUCTION

The recent discovery of high-temperature superconductivity in *RE*FeAsO (Ref. 1) pnictides (1111 family) has triggered the attention of a huge community of solid-state physicists and chemists, who are working extensively on these new phases in order to both increase their critical temperature (T_C) and understand the basic mechanism for superconductivity.[2–5] One way which is being recently investigated in order to promote the insurgence of a superconducting state in 1111 and 122 iron pnictides deals with chemical doping on the Fe site. For these new systems this allows a direct doping on the Fe-As layers opposite to the cuprates HTSC (high temperature superconductors) where charge carriers had to be introduced by doping in the charge-reservoir layers. In addition, by doping the Fe site the role of chemical disorder and chemical pressure on the tetrahedral network can be explored. Replacing Fe ions with 3*d* metal ions such as Co or Ni led to the discovery of new superconducting phases.[6–12] The influence of the *d*-orbitals nature of transition-metal (*TM*) ions has been also explored by means of 4*d* and 5*d* elements doping.[9,10,13] Overall, all these works highlighted the promotion of a superconducting state in F-undoped systems when *TM* ions were introduced on the Fe site. Critical temperatures (T_C) of doped samples vary from ~6 K for the $LaFe_{1-x}Ni_xAsO$ system[8] to ~16 K for the $SmFe_{1-x}Ir_xAsO$ system.[10] The role of doping atoms on the insurgence of superconductivity has not yet been properly described within a theoretical framework. Most of the reported papers suggest that a structural effect on the Fe-As tetrahedral array coupled to the specific electronic structure of the doping elements should be two significant sources of the observed superconductivity.[11] In addition, one of the most prominent effect is correlated with charge doping induced by aliovalent cation replacement together with chemical pressure that should suppress the nesting of electron and hole Fermi surfaces (typical of the undoped systems) and the spin-density wave state thus promoting the insurgence of superconductivity.[14,15]

In this paper we present the results of a synchrotron x-ray diffraction investigation coupled to magnetometry and Raman spectroscopy study on the $SmFe_{1-x}Ir_xAsO$ system ($x=0-0.275$). This solid solution has been selected due to the fact that this system shows the highest T_C among all the F-undoped 1111 iron pnictides investigated so far thus suggesting that this can be a promising playground in order to further enhance the critical temperature. In addition, compared to other systems, the range of Ir doping where superconductivity is observed is the largest one so a thorough structural investigation on $SmFe_{1-x}Ir_xAsO$ samples may lead to important conclusions on the role of cation doping in these systems. The trend of T_C against the Ir doping has a plateau-like behavior which has still to be understood. Finally we put strong efforts in order to study the low Ir-doping region in order to follow the evolution of the orthorhombic-to-tetragonal phase transition present in the SmFeAsO compound as a function of metal doping. Starting from the experimental data collected on this system we developed a general model in order to describe the phase diagrams of *TM*-doped iron pnictide showing which is the key parameter in affecting the properties of such Fe-site-doped pnictides.

II. EXPERIMENTAL

Polycrystalline samples with nominal composition $SmFe_{1-x}Ir_xAsO$ ($0 \leq x \leq 0.275$) were synthesized by conven-

tional solid-state reactions using high-purity SmAs, Ir, Fe, and Fe_2O_3 according to synthesis procedures employed before in our group.[16,17] Each sample batch was about 500 mg. SmAs was prepared starting from Sm rods (NewMetals >99.9%) from which Sm powder was obtained working in glove-box under Ar flux. Pellets of SmAs were prepared and fired at 500 °C for 2 h and then to 900 °C for 18 h in quartz tubes sealed under vacuum ($\sim 10^{-5}$ bar). The reagents were mixed, pressed in form of pellets, wrapped in tantalum foils and left to react at 1160 °C for 48 h in vacuum-sealed quartz tubes ($\sim 10^{-5}$ bar). The samples were characterized by laboratory powder x-ray diffraction at room temperature, synchrotron x-ray diffraction as a function of temperature ($300 \leq T \leq 4$ K) and dc magnetization measurements.

For the synchrotron x-ray diffraction measurements, the $SmFe_{1-x}Ir_xAsO$ ($0 \leq x \leq 0.275$) samples were sealed in borosilicate capillaries (0.5 mm diameter) and measured at a wavelength of $\lambda = 0.399792$ Å at selected temperature points from room temperature down to 4 K on the high-resolution powder diffractometer beamline ID31 at ESRF (Grenoble). Data analysis was performed by Rietveld analysis. Samples were spun on the axis of the diffractometer to reduce any preferred orientation and packing effects.

Raman spectra were measured in backscattering geometry using a confocal micro-Raman spectrometer equipped with a 632.8 nm laser and a charge coupled device detector. The use of a 100× objective allowed a sample area (≈ 2 μm^2) to carefully select on which the laser beam was focused. In order to prevent sample heating the laser power on the sample was kept around 2 mW.[18] Since SmOFeAs is a very poor Raman scatterer,[19] spectra with a good signal-to-noise ratio were collected within the 100–600 cm^{-1} range by setting long acquisition times (120 s) and a large number of spectra were averaged (10).

III. RESULTS

A. Synchrotron x-ray diffraction

According to room-temperature synchrotron x-ray diffraction data for the $SmFe_{1-x}Ir_xAsO$ ($0 \leq x \leq 0.275$) samples all the investigated compositions possess a tetragonal structure (space group $P4/nmm$) at room temperature. Close inspection of the patterns reveal that the samples quality is high with, in some cases, detectable impurities which are always below ~3%. Nominal compositions agree well with the compositions estimated from the refinement of Ir/Fe occupancies within the standard deviation.

Figure 1 reports, as a selected example, a typical Rietveld refinement of an experimental diffraction pattern (in particular the figure refers to the $x=0.275$ sample). Figure 2 shows the trend of lattice parameters $a(b)$ and c as a function of Ir doping at 295 K. A clear expansion of the $a(b)$ parameters occurs coupled to a more significant compression of the c parameter. These results corroborate with previous structural data reported by Chen *et al.*[10] Detailed structural results obtained from the refinement at room temperature are reported in Table I. Interestingly, the cell volume does not show any sensible variation within the broad Ir-doping range explored with a possible trend toward a slight expansion from

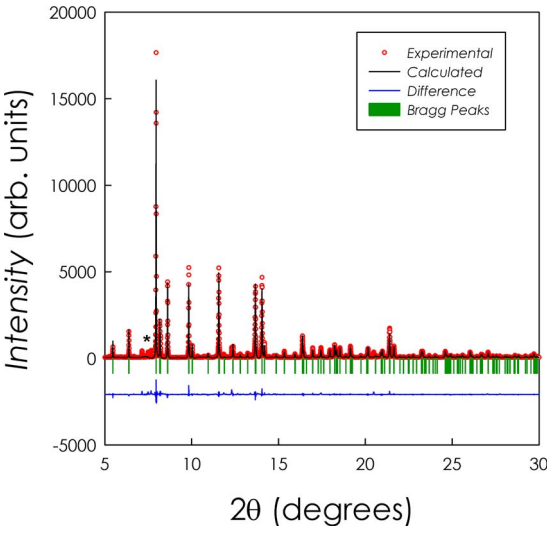

FIG. 1. (Color online) Rietveld refined pattern of $SmFe_{0.725}Ir_{0.275}AsO$ at room temperature. The red empty circles (black empty circles) represent the experimental pattern, the black line the calculated pattern, the blue (black) horizontal line the difference, and the vertical green (black) bars at the bottom of the pattern are the Bragg peaks positions for the refinement.

131.955(6) $Å^3$ for $x=0$ to 132.154(6) $Å^3$ for $x=0.275$ (see Table I).

Figure 3 reports the patterns collected at 30 K on the $SmFe_{1-x}Ir_xAsO$ ($0 \leq x \leq 0.275$) samples in selected 2θ regions. It is clear that low Ir-doped samples ($x=0$, 0.03, 0.04) present a peak splitting at this temperature while samples above $x=0.06$ have a single peak. This peak splitting comes from the presence of an orthorhombic distortion (space group, s.g., *Cmma*) which has previously been observed in several members of the 1111 iron pnictides. In particular, panel (A) of Fig. 3 shows the splitting of the tetragonal (111) reflection to (021) and (201) reflections in the

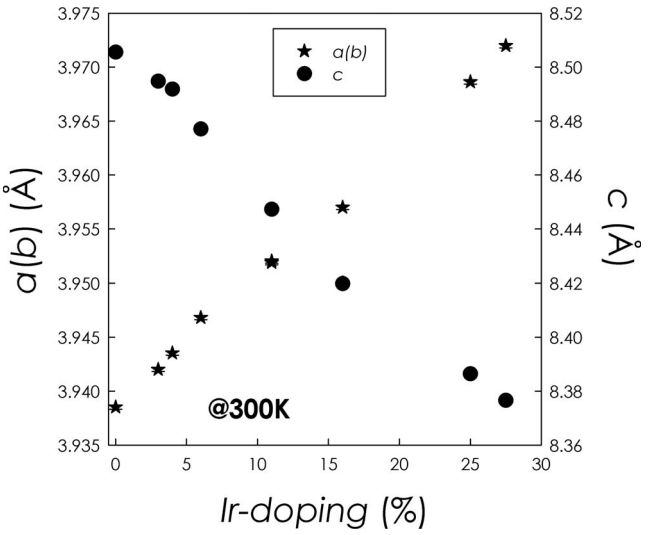

FIG. 2. Lattice parameters vs Ir content for the $SmFe_{1-x}Ir_xAsO$ solid solution ($0 \leq x \leq 0.275$) at 295 K.

TABLE I. Structural parameters for the $SmFe_{1-x}Ir_xAsO$ samples at 295 K.

Ir doping (x)	0	0.03	0.04	0.06	0.11	0.16	0.25	0.275
a,b (Å)	3.93676(2)	3.94201(1)	3.94354(1)	3.94682(2)	3.95187(6)	3.957011(3)	3.968623(8)	3.97195(1)
c (Å)	8.51422(7)	8.49475(3)	8.49182(5)	8.47704(6)	8.44725(2)	8.433563(2)	8.38642(3)	8.37662(4)
	131.955(6)	132.003(5)	132.059(6)	132.050(6)	132.036(6)	132.051(5)	132.086(6)	132.154(6)
z Sm	0.1371(3)	0.1373(1)	0.1370(2)	0.1377(2)	0.1371(1)	0.1369(2)	0.1368(1)	0.1367(2)
z As	0.6623(6)	0.6607(3)	0.6607(4)	0.6623(4)	0.6612(2)	0.6609(2)	0.6603(2)	0.6604(4)
Fe-As (Å)	2.405(3)	2.3971(3)	2.3979(4)	2.4057(2)	2.3997(6)	2.3975(8)	2.3968(9)	2.3978(7)
As-Fe-As (deg)	109.86(8)	110.59(5)	110.63(7)	110.23(7)	110.85(3)	111.27(7)	111.77(3)	111.84(6)
As-Fe-As (deg)	109.3(2)	108.9(1)	108.9(1)	109.1(1)	108.8 (1)	108.6(1)	108.34(7)	108.3 (1)

orthorhombic structure. Panel (B) shows the splitting of the tetragonal reflection (220) to (040) and (400) reflections of the orthorhombic structure.

The sample with $x=0.06$ has a clear asymmetric peak shape as can be inferred from Fig. 3 even though a splitting cannot be resolved as in samples with $x<0.06$. As a matter of fact, a suitable Rietveld refinement of this composition could be achieved again by considering the *Cmma* orthorhombic space group with final lattice parameters at 30 K of $a=5.5717(4)$ Å, $b=5.5806(4)$ Å, and $c=8.4419(8)$ Å. As can be appreciated, the orthorhombic distortion is very small but detectable thanks to the high-resolution data collected on the samples. We stress that this peak asymmetry, indicative of a reduced symmetry, is clearly visible in the patterns of the $x=0.06$ sample at 5 and 30 K while symmetric peaks are found at the next temperature measured, i.e., 100 K. Figure 4 shows the trend of a, b, and c lattice parameters at 5 K as a function of Ir doping.

From the structural data obtained by means of Rietveld refinement we determined the bond-length and bond-angle values as a function of Ir doping at 300 and 5 K which are plotted in Figs. 5 and 6. As can be appreciated the Fe-As bond length does not substantially change along with the Ir doping at both temperatures while the α and β As-Fe-As angles significantly move from their initial values at $x=0$. For the bond angles, the comparison of RT and 5 K data indicates that the α As-Fe-As angle is more affected by the temperature lowering as can be appreciated by the significant increase of the angle value passing from RT to 5 K.

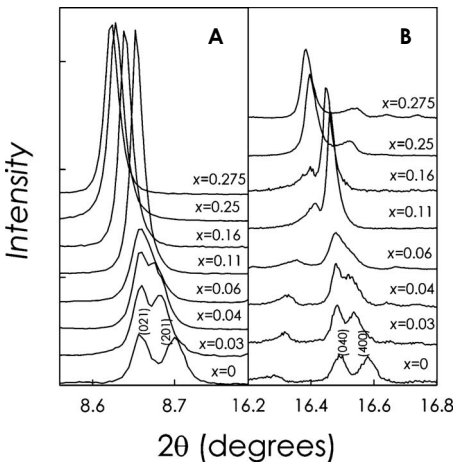

FIG. 3. Synchrotron x-ray patterns collected at 30 K on the $SmFe_{1-x}Ir_xAsO$ ($0\leq x\leq 0.275$) samples in selected 2θ regions.

B. Magnetic properties

The samples investigated in this work have been measured by means of superconducting quantum interference device magnetometry in order to study their superconducting properties. Figure 7 shows the magnetic response of the samples in a 5 G field (field-cooling measurements). Samples with $x=0.06$, 0.11, and 0.16 have clear superconducting transitions with a T_C of 18.0 K at $x=0.06$, 18.3 K at $x=0.11$, and 17.3 K at $x=0.16$. Superconducting fraction increases with x and reaches a maximum at $x=0.11$. Samples with $x<0.06$ are not SC (superconducting) and with a clear antiferromagnetic transition (see, for example, the curve of Fig. 7 for $x=0.04$, zero-field-cooling and field-cooling measurements, in this case) while samples with $x>0.16$ are not superconducting without any sign of long-range magnetic order. A possible very small SC fraction can be detected in the $x=0.25$ sample even though the bulk of the sample is not SC.

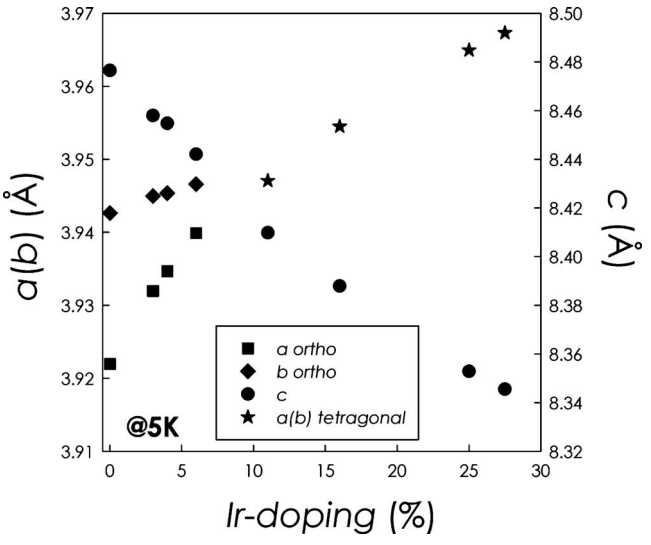

FIG. 4. Lattice parameters vs Ir content for the $SmFe_{1-x}Ir_xAsO$ solid solution ($0\leq x\leq 0.275$) at 5 K. a and b lattice parameters in the orthorhombic structure have been divided by $\sqrt{2}$.

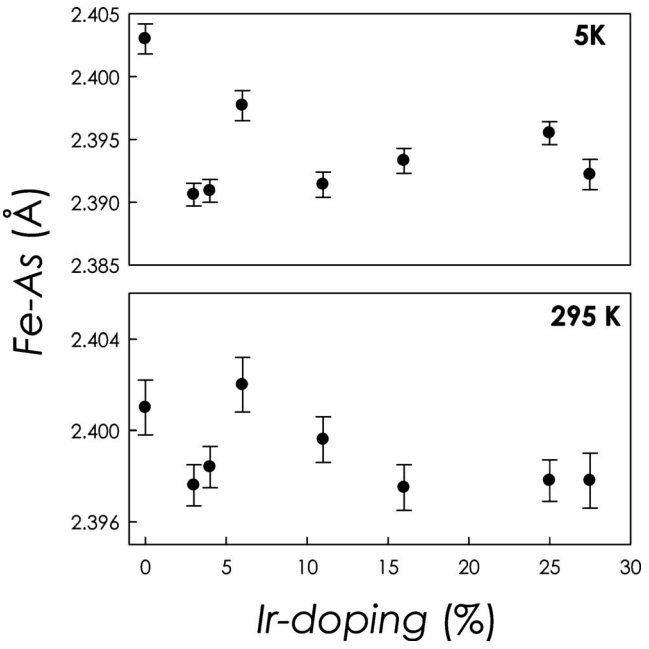

FIG. 5. Fe-As bond length vs Ir content for the $SmFe_{1-x}Ir_xAsO$ solid solution ($0 \leq x \leq 0.275$) at 295 and 5 K.

C. Raman spectroscopy

The pure and the Ir-doped samples have been investigated by means of micro-Raman spectroscopy to verify the chemical homogeneity of the sample over the micron scale and to study the effects of the Ir doping on the lattice dynamics. All the Raman spectra collected from several points of the $x=0$ sample showed the three dominant lines at 170, 200, and 210 cm^{-1} [see Fig. 8(a)], already observed in previous Raman studies.[19,20] The 170 cm^{-1} line is due to a phonon mode

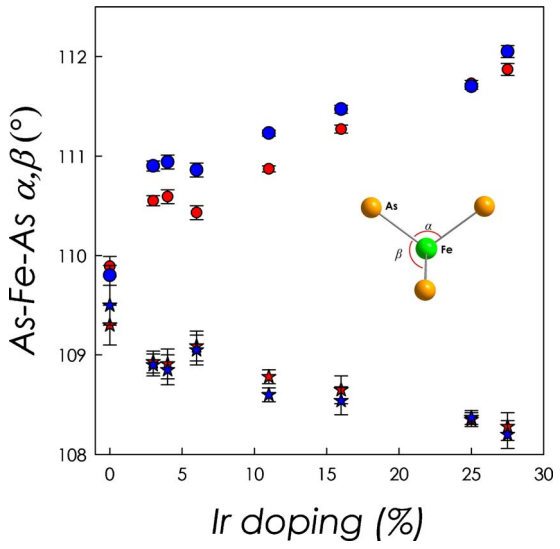

FIG. 6. (Color online) As-Fe-As bond angles (α and β) vs Ir content for the $SmFe_{1-x}Ir_xAsO$ solid solution ($0 \leq x \leq 0.275$) at 295 and 5 K. Red (light gray) and blue (dark gray) circles represent the α angles at 295 K and 5 K, respectively. Red (light gray) and blue (dark gray) stars represent the β angles at 295 K and 5 K, respectively.

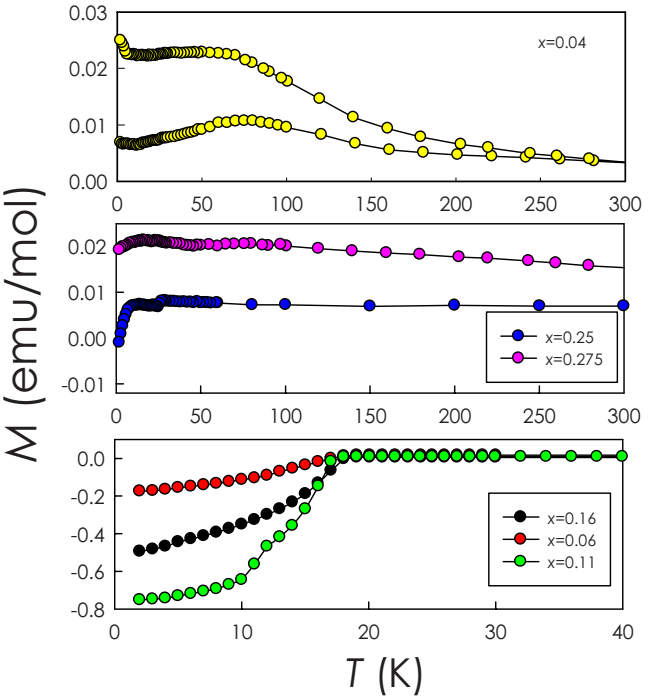

FIG. 7. (Color online) Magnetization data at 5 G for the $SmFe_{1-x}Ir_xAsO$ solid solution ($0 \leq x \leq 0.275$).

of A_{1g} symmetry (mainly involving Sm atoms), the 200 cm^{-1} to a phonon of A_{1g} symmetry (As atoms), and the 210 cm^{-1} line to a phonon of B_{1g} symmetry (Fe atoms). The absence of other spurious peaks allows us to rule out the presence of detectable amount of impurities (e.g., samarium oxide), previously evidenced in SmFeAsO samples by Raman spectroscopy.[20] We notice that Raman spectra collected at different points on the sample surface can show different relative intensities of the phonon peaks [see the spectra labeled P1 and P2 in Fig. 8(a)]. This must be ascribed to polarization effects, since the intensity of the Raman peaks can depend on the angle between the laser polarization and the possible preferred orientation of the crystallites in the scattering volume.

Typical Raman spectra collected on the Ir-doped samples ($x=0.06$, 0.11, 0.25, and 0.275) are also reported in Fig. 8(a). On increasing the Ir content, disorder increases in the solid solution, and the Raman lines decrease in intensity and broaden. In particular, it is no longer possible to resolve the two lines at 200 and 210 cm^{-1} and at $x=0.275$ the measured Raman signal becomes very low and only poor-quality spectra can be obtained. As to the peak frequencies ω_i, no significant change occurs on increasing the Ir content, as shown in Fig. 8(b) where the ω_i values resulting from a standard line-shape analysis of a large number of spectra are reported. In particular, the peak frequency of the line due to the B_{1g} mode involving Fe atoms does not appreciably change when the heavier Ir substitutes Fe. This behavior shows, on one hand, that the lattice dynamics of the Fe-As atoms are not remarkably affected by Ir doping and, on the other hand, bearing in mind that phonon line arises from a collective excitation of an ordered network, that a sufficiently long-range order is not established even in the solid solution with 27.5% of Ir atoms.

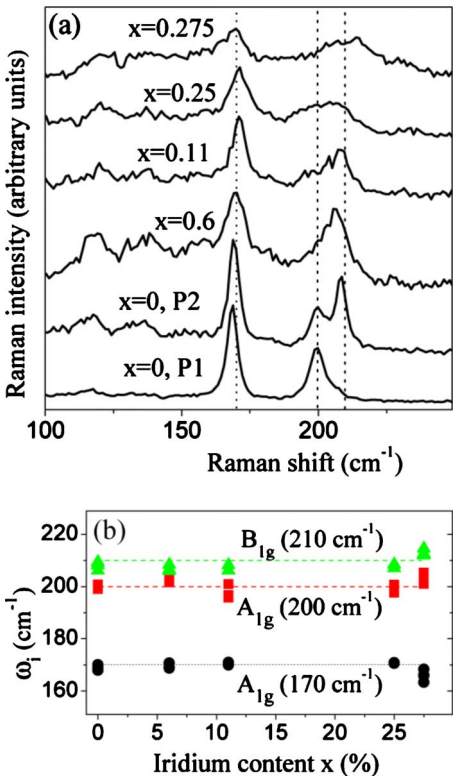

FIG. 8. (Color online) (a) Typical Raman spectra collected on the $x=0$, 0.06, 0.11, 0.25, and 0.275 samples. In the $x=0$ case, spectra collected in two different points (P1 and P2) are shown. Vertical dashed lines mark the frequency of the three dominant Raman lines (170, 200, and 210 cm^{-1}). (b) Peak frequency values ω_i resulting from a standard line-shape analysis of a large number of measured spectra, as a function of the Ir content x.

IV. DISCUSSION

The study of *TM*-doped 1111 iron pnictides is of great interest since it may shed further light on the relative role of structure and doping on the physical properties of these new systems. Ir doping in the SmFeAsO lattice gives origin to the formation of a solid solution as witnessed by the linear change of lattice parameters. The doping with Ir leads also to the disappearance (for $x>0.06$) of the tetragonal-to-orthorhombic ($T\rightarrow O$) transition found in the parent compound SmFeAsO and to the insurgence of a SC state, thus making the system to evolve in an analogous way as the F doping. As a matter of fact, Ir has a stable oxidation state higher than Fe^{2+} and this implies that an aliovalent cation substitution on the Fe site has, in terms of charge balance, the analogous effect of F doping on the O site. However, several differences between the two kinds of doping are clearly visible. From the point of view of T_C, once the threshold for the insurgence of the superconducting state has been reached (in the present case $x=0.06$) the critical temperature has no substantial dependence with the Ir doping (and consequently on the charge-carrier doping). Another interesting feature is that the maximum T_C is already observed at $x=0.06$, that is in a sample which is orthorhombic in the temperature range of the insurgence of the superconducting state and the T_C is significantly lower with respect to that expected by a similar charge doping due to fluorine substitution for oxygen. In addition, the trend of Raman modes suggests that electronic effects do not take a strong part in the evolution of the phonon spectra with Ir doping.

If we look at the trend of bond angles, it is possible to observe that the tetrahedral (α) angle (at RT) moves from $\sim 110°$ at $x=0$ to $\sim 111.9°$ at $x=0.275$. It is well known that a close correlation exists between the value of this angle (at RT) and the T_C with maximum critical temperatures found in correspondence of the "ideal" tetrahedral angle of 109.4°. However, if one compares the range of α values where superconductivity emerges[21] it is clear that, just considering this structural parameter, all the composition of the $SmFe_{1-x}Ir_xAsO$ solid solution are well within the range where T_C above 20–30 K should be observed. This result is a clear demonstration that this simple structural dependence of iron pnictides physical properties does not hold in Fe-site-substituted samples, even for an analogous charge doping. The system we have chosen is even more suitable to such a demonstration since the Fe(Ir)-As average bond length has minimal variation with doping. Also the absence of a maximum T_C for angles closer to the tetrahedral value suggests that other parameters affect the insurgence and dependence of critical temperature with doping.

Further insight on the behavior of *TM*-doped iron pnictides can be inferred from a comparison with other doped phases. Very recently, a deep and thorough investigation on the $NdFe_{1-x}Co_xAsO$ solid solution has been reported.[22] A close inspection of the experimental results on this system shows a number of quite remarkable similarities with the data reported in this work. For example, the range of Co doping where superconductivity emerges resembles very closely the one of the $SmFe_{1-x}Ir_xAsO$ system as well as for the trend in bond angles and other structural parameters such as the region of $T\rightarrow O$ transition existence. However, the two systems—apart for the different *RE*—contain either a 3*d* (Co) or 5*d* (Ir) element and as a consequence more significant differences should be expected if the electronic properties of the transition metal are the essential ingredient in determining the physical properties of Fe-site-doped systems. Other compositions such as $LaFe_{1-x}Ir_xAsO$ show a maximum T_C for $x\sim 0.075$ (11.8 K) while $LaFe_{1-x}Ni_xAsO$ presents the maximum critical temperature for a very low doping of about 0.04 ($T_C=6.1$ K).

Overall, one can make use of all the available experimental data on *TM*-doped iron pnictides and try to look for meaningful correlations. Figure 9 [panel (A)] reports the trend of critical temperatures as a function of c/c_0 (chosen as relevant parameter for the reason explained below) for all the available doped samples of the $LaFe_{1-x}TM_xAsO$ system (Refs. 1–7). c/c_0 has been calculated as the ratio between the c-axis value for the *TM*-undoped sample and the c value at a defined doping. We highlight that the data plotted in this figure are those related to compositions, within each $LaFe_{1-x}TM_xAsO$ solid solution, displaying the maximum T_C. As can be appreciated from the plot, a good correlation exists between the compressibility induced on the c axis by the *TM* doping and the critical temperature. As a matter of fact, all these doped samples show huge variations of the c axis along with doping levels while the a axis remains only slightly

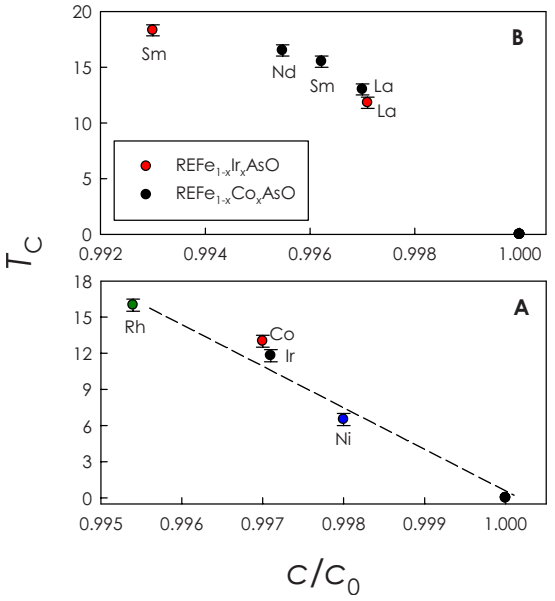

FIG. 9. (Color online) Panel (A): the trend of critical temperatures as a function of c/c_0 for several doped samples of the $LaFe_{1-x}TM_xAsO$ system (Refs. 1–7). Panel (B): T_C vs c/c_0 for distinct $REFe_{1-x}TM_xAsO$ systems (TM=Co and Ir) (Refs. 4–7).

doping dependent. This correlation seems to be solid irrespective to the fact that some of the dopant ions could lead to a charge doping due to the difference in the valence state between the Fe and *TM* ion (but, unfortunately, up to now no systematic x-ray absorption spectroscopy investigation of doped samples has been carried out in the literature—future measurements of this kind on several systems are planned). The use of c/c_0 parameter has been chosen in order first to mimic the effect of an applied external pressure and then because the actual ion size of *TM* dopants is not well known due to the lack of information regarding their oxidation state. For the $LaFe_{1-x}TM_xAsO$ solid solution the T_C increases from about 6 K (Ni doping)[8] to 16 K (Rh doping)[9] as the c/c_0 values reduces. Interestingly, in the undoped LaFeAsO system, a superconducting state ($T_C \approx 13.5$ K) is induced by an external pressure of about 1.7 GPa,[23] then a maximum T_C of about 20 K is observed around 5 GPa with T_C staying constant up to 20 GPa before the critical temperature starts decreasing. This results in a T_C vs P phase diagram with a typical dome shape which is actually found in all the undoped or lightly F-doped samples of the iron pnictide family. We stress here that this is also the typical shape found in the phase diagrams of all the *TM*-doped (F-undoped) iron pnictides. If structural data as a function of pressure for the LaFeAsO system were available, one could try to compare the effect of a hydrostatic pressure (which actually acts also on the *a*-axis compressibility even though in a less pronounced way with respect to the *c* axis) to that of the chemical pressure (substantially only effective on the *c* direction) induced by the chemical doping on the Fe site.

An additional evidence of this chemical pressure effect induced by the *TM* doping on the Fe site can be inferred by looking at Fig. 9 [panel (B)]. In this case we have plotted the T_C vs c/c_0 for distinct $REFe_{1-x}TM_xAsO$ systems keeping constant the *TM* dopant and showing the dependence with the *R*. This is a more expected correlation related to the increase of T_C with reduction of the *R*-site volume which mimics the external pressure. The robustness of the correlation is further appreciable due to the fact that we are plotting samples with variable concentrations of *TM* ions which show the maximum T_C within their specific $REFe_{1-x}TM_xAsO$ solid solution.

As we already pointed out above, the classical dome-shaped T_C vs x phase diagram found in *TM*-doped iron pnictides may be substantially correlated with the lattice compression induced by the doping element. By increasing chemical pressure (as occurs with hydrostatic pressure) the critical temperature passes through a more or less pronounced dome-shaped phase diagram and then decreases and vanishes. Very recently it has been suggested that in underdoped iron pnictides the application of an external pressure favors the setup of antiferromagnetic fluctuations which predominates at high pressure and would suppress development of superconductivity, namely, remarkable enhancement of T_C.[24] Interestingly, *TM* overdoped *RE*FeAsO samples become antiferromagnetic.[22]

V. CONCLUSION

In this paper we have carefully investigated the structural and physical properties of the $SmFe_{1-x}Ir_xAsO$ solid solution ($0 \leq x \leq 0.275$) chosen as a case study. Our data confirms the positive role of doping in terms of insurgence of superconductivity and suppression of the $T \rightarrow O$ transition. Increasing doping levels lead to the disappearance of superconductivity while preserving the tetragonal structure, despite As-Fe(Ir)-As bond angles within the range where superconductivity should be observed. The set of data collected in this paper have been used together with available literature results on similar *TM*-doped *RE*FeAsO compounds in order to try to understand the peculiar behavior of these phases. A possible explanation based on a pure chemical pressure effect has been proposed and corroborated by experimental data. Based on these observations, further experimental and theoretical works seem highly desirable and urgently needed.

ACKNOWLEDGMENTS

We gratefully acknowledge funding from CARIPLO Foundation (Project No. 2009-2540 "Chemical Control and Doping Effects in Pnictide High-temperature Superconductors") and the ESRF for providing beam time.

*Corresponding author. FAX: +39-(0)382-987575; lorenzo.malavasi@unipv.it

[1] Y. Kamihara, T. Watanabe, M. Hirano, and H. Hosono, J. Am. Chem. Soc. **130**, 3296 (2008).
[2] H. Luetkens, H.-H. Klauss, M. Kraken, F. J. Litterst, T. Dellmann, R. Klingeler, C. Hess, R. Khasanov, A. Amato, C. Baines, M. Kosmala, O. J. Schumann, M. Braden, J. Hamann-Borrero, N. Leps, A. Kondrat, G. Behr, J. Werner, and B. Büchner, Nature Mater. **8**, 305 (2009).
[3] A. J. Drew, Ch. Niedermayer, P. J. Baker, F. L. Pratt, S. J. Blundell, T. Lancaster, R. H. Liu, G. Wu, X. H. Chen, I. Watanabe, V. K. Malik, A. Dubroka, M. Rössle, K. W. Kim, C. Baines, and C. Bernhard, Nature Mater. **8**, 310 (2009).
[4] J. Zhao, Q. Huang, C. de la Cruz, S. Li, J. W. Lynn, Y. Chen, M. A. Green, G. F. Chen, G. Li, Z. Li, J. L. Luo, N. L. Wang, and P. Dai, Nature Mater. **7**, 953 (2008).
[5] G. Lang, H.-J. Grafe, D. Paar, F. Hammerath, K. Manthey, G. Behr, J. Werner, and B. Büchner, Phys. Rev. Lett. **104**, 097001 (2010).
[6] C. Wang, Y. K. Li, Z. W. Zhu, S. Jiang, X. Lin, Y. K. Luo, S. Chi, L. J. Li, Z. Ren, M. He, H. Chen, Y. T. Wang, Q. Tao, G. H. Cao, and Z. A. Xu, Phys. Rev. B **79**, 054521 (2009).
[7] A. S. Sefat, A. Huq, M. A. McGuire, R. Jin, B. C. Sales, D. Mandrus, L. M. D. Cranswick, P. W. Stephens, and K. H. Stone, Phys. Rev. B **78**, 104505 (2008).
[8] G. Cao, S. Jiang, X. Lin, C. Wang, Y. Li, Z. Ren, Q. Tao, C. Feng, J. Dai, Z. Xu, and F.-C. Zhang, Phys. Rev. B **79**, 174505 (2009).
[9] S. Muir, A. W. Sleight, and M. A. Subramanian, Mater. Res. Bull. **45**, 392 (2010).
[10] Y. L. Chen, C. H. Cheng, Y. J. Cui, H. Zhang, Y. Zhang, Y. Yang, and Y. Zhao, J. Am. Chem. Soc. **131**, 10338 (2009).
[11] S. A. J. Kimber, A. Kreyssig, Yu.-Z. Zhang, H. O. Jeschke, R. Valentí, F. Yokaichiya, E. Colombier, J. Yan, T. C. Hansen, T. Chatterji, R. J. McQueeney, P. C. Canfield, A. I. Goldman, and D. N. Argyriou, Nature Mater. **8**, 471 (2009).
[12] P. L. Alireza, Y. T. C. Ko, J. Gillett, C. M. Petrone, J. M. Cole, G. G. Lonzarich, and S. E. Sebastian, J. Phys.: Condens. Matter **21**, 012208 (2009).
[13] Y. Qi, L. Wang, Z. Gao, D. Wang, X. Zhang, Z. Zhang, and Y. Ma, EPL **89**, 67007 (2010).
[14] C. de la Cruz, Q. Huang, J. W. Lynn, J. Li, W. Ratcliff II, J. L. Zarestky, H. A. Mook, G. F. Chen, J. L. Luo, N. L. Wang, and P. Dai, Nature (London) **453**, 899 (2008).
[15] T. J. Liu, J. Hu, B. Qian, D. Fobes, Z. Q. Mao, W. Bao, M. Reehuis, S. A. J. Kimber, K. Prokeš, S. Matas, D. N. Argyriou, A. Hiess, A. Rotaru, H. Pham, L. Spinu, Y. Qiu, V. Thampy, A. T. Savici, J. A. Rodriguez, and C. Broholm, Nature Mater. **9**, 718 (2010).
[16] G. A. Artioli, L. Malavasi, M. C. Mozzati, and Y. Diaz-Fernandez, J. Am. Chem. Soc. **131**, 12044 (2009).
[17] L. Malavasi, G. A. Artioli, C. Ritter, M. C. Mozzati, B. Maroni, B. Pahari, and A. Caneschi, J. Am. Chem. Soc. **132**, 2417 (2010).
[18] A. Paolone, A. Sacchetti, T. Corridoni, P. Postorino, and R. Cantelli, Solid State Ionics **170**, 135 (2004).
[19] V. G. Hadjiev, M. N. Iliev, K. Sasmal, Y. Y. Sun, and C. W. Chu, Phys. Rev. B **77**, 220505 (2008).
[20] C. Marini, C. Mirri, G. Profeta, S. Lupi, D. Di Castro, R. Sopracase, P. Postorino, P. Calvani, A. Perucchi, S. Massidda, G. M. Tropeano, M. Putti, A. Martinelli, A. Palenzona, and P. Dore, EPL **84**, 67013 (2008).
[21] K. Ishida, Y. Nakai, and H. Hosono, J. Phys. Soc. Jpn. **78**, 062001 (2009).
[22] A. Marcinkova, D. A. M. Grist, I. Margiolaki, T. C. Hansen, S. Margadonna, and Jan-Willem G. Bos, Phys. Rev. B **81**, 064511 (2010).
[23] H. Takahashi, H. Okada, K. Igawa, Y. Kamihara, M. Hirano, H. Hosono, K. Matsubayashi, and Y. Uwatoko, J. Supercond. Novel Magn. **22**, 595 (2009).
[24] T. Nakano, N. Fujiwara, K. Tatsumi, H. Okada, H. Takahashi, Y. Kamihara, M. Hirano, and H. Hosono, Phys. Rev. B **81**, 100510(R) (2010).